

A first-principles study of wurtzite-structure MnO

P. Gopal and Nicola A. Spaldin
Materials Department, University of California,
Santa Barbara, CA 93106-5050.

Umesh V. Waghmare
Theoretical Sciences Unit,
Jawaharlal Nehru Centre for Advanced Scientific Research,
Bangalore, 560 064 INDIA

November 14, 2018

Abstract

We present results of a density functional theory study of MnO in the wurtzite structure. Our motivation is provided by recent experiments reporting ferromagnetism in Mn-doped wurtzite-structure ZnO. We find that wurtzite MnO a) is not strongly energetically disfavored compared with the ground state rocksalt MnO, b) shows strong magneto-structural coupling and c) has a piezoelectric response that is larger than that of ZnO. These predictions augur well for the creation of ferromagnetic piezoelectric semiconductors based on Mn-doped ZnO.

1 Introduction

The wurtzite structure adopted by ZnO does not have a center of inversion symmetry and therefore permits the occurrence of piezoelectricity. Indeed previous studies have revealed that the ZnO piezoelectric coefficients are substantial [1] because of incomplete cancellation between opposing ionic and electronic contributions [2, 3]. ZnO is already widely used in varistors for surge protection and as filters for incoming television signals. The large piezoelectric response might provide improved electronic device performance, for example, enhanced and tunable optical devices and optical wave resonators.

Additional interest in ZnO-based systems has recently been stimulated by predictions of ferromagnetism in transition metal-doped ZnO using a simple mean field model [4] and also by density functional methods [5, 6]. Numerous experimental reports of ferromagnetism [7, 8, 9, 10, 11] including some above room temperature [12] have also appeared. Although more recent experimental [13] and theoretical [14] studies call these earlier observations into question, there is a clear need for further research in this field.

In this paper we investigate the fundamental question of what happens to the piezoelectric response when Mn is substituted for Zn in the wurtzite structure. The answer is not obvious; some wurtzite materials, such as BeO, do not show a large piezoelectric response even though it is allowed by the non-centrosymmetry of the crystal structure. The situation is even more complicated in the case of transition-metal substituents because of the availability of partially-filled $3d$ states which can become involved in chemical bonding. Such states have been shown to strongly suppress the occurrence of ferroelectricity [15], but their influence on piezoelectricity has not been previously investigated. We choose Mn as our model transition metal dopant because the $3d$ band of the Mn^{2+} ion is exactly half-filled, with a gap between the up-spin occupied states and empty down-spin states. Therefore we

anticipate a more straightforward band structure than in the case of other transition metals in which one of the bands is usually partially filled. Also, such an arrangement is more likely to result in an insulating state, which is a prerequisite for the occurrence of piezoelectricity.

Our primary finding is that wurtzite MnO in fact has a larger piezoelectric response than ZnO by upto around 3 times. This remarkable result suggests that, in addition to being ferromagnetic, transition metal doped ZnO should have a strong piezoelectric response. Device applications that have been suggested for such magnetic piezoelectrics, include variable transducers with magnetically-tunable piezoelectricity, and electric field or stress-controlled ferromagnetic resonance devices[16]. Also, the ability to couple with *either* the magnetic *or* the electric polarization will offer an extra degree of freedom in the design of conventional sensors, actuators, transducers and storage devices. The ability to transform changes in the magnetic field into electrical voltage and vice-versa could be used as a magnetic field sensor for magnetic field measurement, or in electric current measurement.

The remainder of this paper is organized as follows. In section II we summarize previous calculations on MnO in the usual rocksalt structure, and compare our own results with those of the literature. In Sec. III we describe the electronic structure of MnO in the wurtzite structure. In Sec. IV we present the results of our studies of magneto-structural coupling and piezoelectricity in wurtzite MnO. In the last section we present our conclusions and suggestions for future work.

2 MnO in the Rocksalt structure

The experimental ground state crystal structure of MnO is rocksalt [17]. In this section we present results of our calculations for rocksalt-structure MnO in three magnetic orderings, namely the ferromagnetic (FM) and two types of anti-ferromagnetic (AFM) orderings. In type-I AFM ordering (AFI), the Mn ions are ferromagnetically aligned in the [001] planes, with adjacent planes aligned antiferromagnetically to each other, while in type-II ordering (AFII) they are ferromagnetically aligned in [111] planes, again with antiferromagnetic alignment between the planes. The type-II structure is the experimentally observed ground state. The purpose of this section is two-fold. First to compare with existing data in order to verify our methodology and pseudopotentials, and second as a point of comparison for our later studies on MnO in the wurtzite structure.

Our total energy calculations were carried out using the local spin density approximation (LSDA) to density functional theory (DFT) [18, 19], with pseudopotentials and a planewave basis as implemented in the ABINIT [20] computer code. We used the optimized pseudopotentials developed by Rappe *et al.*, [21] for both the Mn and the O atoms. Our semi-core Mn pseudopotential was constructed from a $3s^2, 3p^6, 3d^5$ Mn²⁺ valence configuration, with cutoff radii for the s , p and d states of 1.2, 1.1 and 1.4 a.u.s respectively. Optimization of the energy cutoff was carried out using a wave vector, q_c , of 9 a.u.s. with four Bessel functions. The oxygen pseudopotential used a $2s^2, 2p^6$ neutral valence configuration with cutoff radii of 1.2 and 1.4 a.u. for s and p states respectively. Optimization of kinetic energy cutoff for the oxygen states used q_{cs} of 7.0 and 6.5 a.u.s with four and three Bessel functions respectively. Good convergence was obtained with a plane-wave energy cutoff of 82 Ry for these pseudopotentials. Rhombohedral magnetic unit cells, containing two formula units of MnO, were used for all three magnetic configurations. Highly converged special \mathbf{k} -point sets consisting of 216 points in the rhombohedral Brillouin zone were used in each case. The exchange-correlation functional was parameterized using the Perdew-Zunger parameterization [22] of the Ceperley-Alder [23] exchange-correlation functional.

First we optimized the structures for each magnetic ordering and calculated the total energies, which are listed in Table 1. As expected, we found the AFII configuration to be lowest in energy, with the AFI 0.55 eV/formula unit higher, and the FM 0.60 eV/formula unit above AFI. This ordering is consistent with experiment [17], first-principles Hartree Fock calculations [24] and previous LSDA density functional calculations [25, 26, 27]. Our

Magnetic ordering	Energy (eV/formula unit)
AFII	0.00
AF1	0.55
FM	0.61

Table 1: Relative energies of different magnetic configurations in rocksalt-structure MnO

optimized rhombohedral lattice constant for AFII MnO was 8.16 a.u., consistent with previous LSDA calculations [28] and showing the typical LSDA underestimation relative to the experimental value of 8.38 a.u. [17].

In Figure 1, we show our calculated band structure of AFII MnO which is calculated at the experimental value of 8.38 a.u. (The zero of energy is set to coincide with the highest occupied orbital). The occupied d states lie at the top of the valence band, and their splitting by the rhombohedral crystal field into two doublets and a singlet can be seen clearly. Below and slightly separated from them are the predominantly oxygen p states which have a band width of around 4.5 eV. We will show later that the bandwidths of the Mn and O bands are affected by both the structure and by the magnetic ordering of the system. We obtain an energy gap of 0.75 eV, in perfect agreement with earlier LDA calculations [28]. Analysis of the orbital character of the LSDA band gap [29] indicates that it lies between predominantly up-spin d states at the top of the valence band, and down-spin d states on the same Mn atom at the bottom of the conduction band.

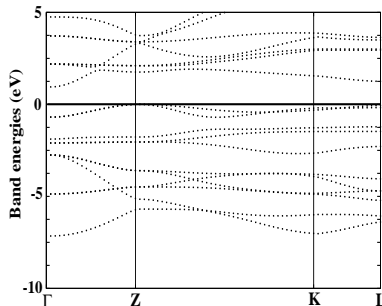


Figure 1: Band structure of AFII MnO plotted along the high symmetry lines of the rhombohedral Brillouin zone.

3 MnO in the wurtzite structure

Having established that our pseudopotentials accurately reproduce previous results for rocksalt-structure MnO, we now turn to the main part of our paper, the study of MnO in the wurtzite structure. As mentioned in the introduction, our motivation is provided by recent experiments in which transition metals are doped into ZnO, where their local environment is the four-fold coordinated structure considered here.

We study the six magnetic orderings of wurtzite MnO shown in Figure 3. (Note that these were previously studied for MnS by Hines et al. [30].) Identical unit cells, containing 8 formula units, were adopted for all structures, and the pseudopotentials and cut-offs were the same as those described in Section 2. A $4 \times 4 \times 4$ \mathbf{k} -point grid was used in all the calculations. A two-dimensional projection of the unit cell, looking down the c axis is shown in Figure 3. The filled circles represent one set of ions in the the $z=0$ and the $z=1$ planes ,

while the empty circles show the positions of the other ions in the $z = \frac{1}{2}$ plane.

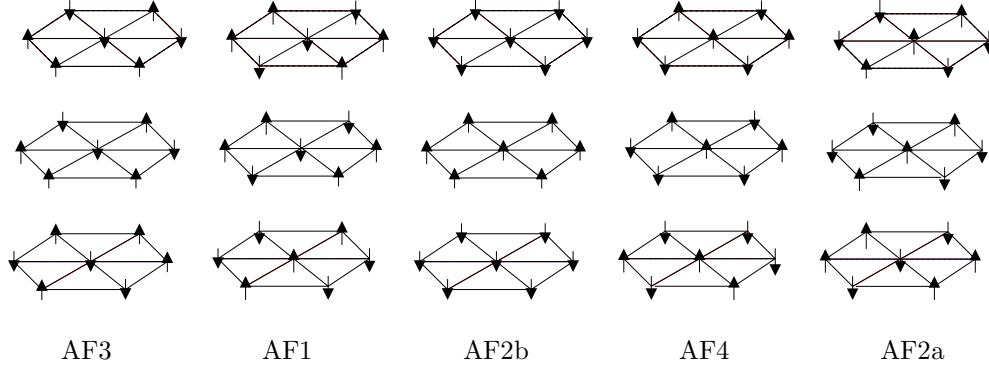


Figure 2: Different magnetic orderings for wurtzite structure MnO studied in this work.

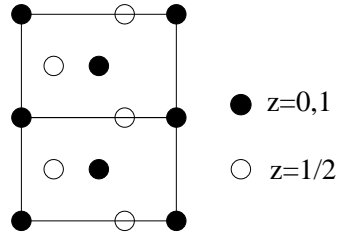


Figure 3: Two-dimensional projection of the unit cell of wurtzite MnO used in this work

4 Energetics

Initially we set the lattice parameters to those of ZnO, and found that the AF3 structure was lowest in energy. However prohibitively large stresses were obtained for all the magnetic orderings at these lattice parameters. Therefore we chose new lattice parameters, a and c of 3.2847 Å and 5.1789 Å (around 1 % larger than the corresponding values in ZnO) and a u value of 0.3687. These new values gave acceptably small stresses. In order to decouple the effects of changes in structure from effects of changes in magnetic ordering, we then calculated the properties of all our magnetic structures at these lattice parameters, and obtained the relative total energies for the wurtzite structures listed in Table 2. The calculated energy ordering is

$$\text{AF3} < \text{AF1} < \text{AF2b} < \text{AF4} < \text{AF2a} < \text{FM}.$$

Note that the energies of the AF3 and AF1 phases are very similar, as are those of the AF2b, AF4 and AF2a. We relate this below to the ferro- and antiferromagnetic interactions between Mn nearest neighbors. As in the rocksalt case, the ferromagnetic phase is highest in energy. It is notable that the relative energies per formula unit of the AF3 wurtzite structure and the AFII rocksalt structure are the same within the errors of the calculations. This suggests that it is not unfavorable to incorporate Mn into a tetrahedral environment.

In Figure 4 we show the band structures for AF3 and FM wurtzite structure MnO (only the up-spin states are shown in the FM case). Note that in both cases we obtain metallic

Magnetic ordering	Energy (eV/formula unit)
AF3	0.000
AF1	0.002
AF2b	0.098
AF4	0.113
AF2a	0.118
FM	0.426

Table 2: Relative energies of the different magnetic orderings in wurtzite MnO. The energies are given relative to the reference lowest energy AF3 structure.

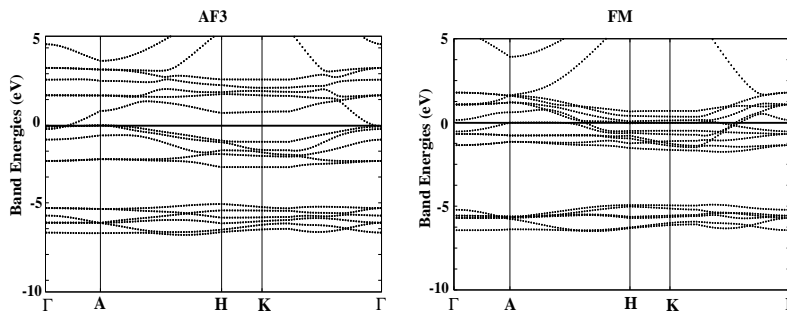


Figure 4: Band structures of wurtzite MnO for AFM (left) and FM (right) orderings, only the up spin states are shown in the FM case.

band structures, with the FM phase having numerous Mn d derived bands crossing the Fermi energy. The AF3 phase (and the other AFM phases, which are not shown) is close to being gapped, with only the Mn $4s$ band crossing the Fermi energy at the Γ point. We point out that the metallicity is an artifact of the underestimation of the gap by the LSDA, and in practice we anticipate that all of the AFM structures should be insulating. Again the top of the valence band is composed of predominantly Mn $3d$ states, which this time show the $e - t_2$ crystal field splitting of the tetrahedral coordination. The predominantly oxygen $2p$ bands are again below the Mn d bands and separated from them by a gap. The bottom of the conduction band is largely composed of Mn $3d$ states, except for the broad $4s$ band that crosses the Fermi energy. Compared with the rocksalt band structure, the bands are narrower, as anticipated for Mn in four-fold rather than six-fold coordination. In addition, it is notable that the wurtzite AFM structure has broader bands than the wurtzite FM. This reflects the increase in hybridization possible, via the usual superexchange interaction, in the AFM bonded configuration. Mn-O hybridization is unfavorable in the FM configuration between d^5 Mn $^{2+}$ ions as a result of Hund's rule. Cartoons of the Mn-O bonding in the AFM and FM cases are shown in Figure 5.

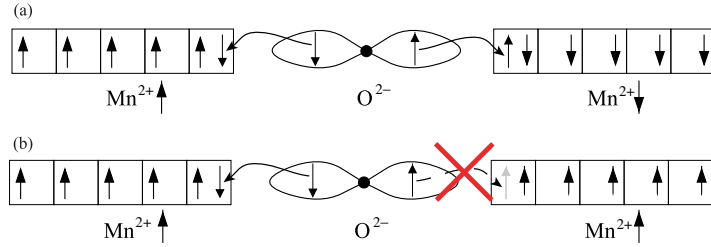


Figure 5: Schematic of (a) favorable Mn-O hybridization in the AFM configuration and (b) unfavorable hybridization in the FM configuration. In (a) the Mn ions are antiferromagnetically coupled. Therefore the down-spin oxygen $2p$ electron undergoes covalent bond formation with an up-spin Mn $3d$ electron (left) leaving an up-spin oxygen $2p$ electron to form a covalent bond with a down-spin Mn $3d$ electron (right). In (b) the Mn ions are ferromagnetically coupled. Therefore if the down-spin oxygen $2p$ electron bonds with an up-spin Mn $3d$ electron on the left (as in the antiferromagnetically coupled case above) the remaining up-spin oxygen $2p$ electron is unable to bond with the *up-spin* Mn $3d$ electrons on the right. Therefore the amount of hybridization, and hence the band width, is reduced in the ferromagnetic case.

4.1 Exchange Couplings

To understand the relative energies of the different spin orderings, we next analyze the energy differences between the configurations using a two-parameter Heisenberg model;

$$H = E_0 + \sum J_{ij} S_i \cdot S_j \quad (1)$$

where $S_i \cdot S_j = +1$ if the spins i and j are parallel, and -1 if they are antiparallel. We include two different values for J ; an in-plane Mn-Mn interaction, J_p , and an out-of-plane (along c) interaction, J_c , as shown in Figure 6. Note that, for the ideal wurtzite structure, the in-plane and out-of-plane Mn-Mn distances are identical, and we would expect to obtain $J_p = J_c$ in the absence of any kind of spin-orbit coupling. However, we constrain the parameter u to be 0.368 which is smaller than the ideal value of 0.375 and hence we find a percentage difference in J_p and J_c of the order of the deviation from the ideal value.

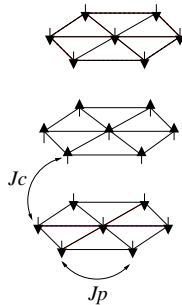


Figure 6: Schematic of the exchange parameters J_p and J_c .

Table 3 gives the number of parallel and antiparallel in-plane and out-of-plane nearest neighbors for a Mn ion in each magnetic structure. Note that the AF3 and AF1 structures have

		AF3	AF1	AF2b	FM	AF4	AF2a
in-plane	$\uparrow\downarrow$	4	4	0	0	4	4
	$\uparrow\uparrow$	2	2	6	6	2	2
out-of-plane	$\uparrow\downarrow$	4	4	6	0	2	2
	$\uparrow\uparrow$	2	2	0	6	4	4

Table 3: Number of in-plane and out-of-plane FM and AFM interactions for each magnetic configuration.

identical types of nearest-neighbor (nn) Mn-Mn interactions (4 in-plane AFM and 4 out-of-plane AFM), which explains their similar energies. Similarly, AF4 and AF2a have identical numbers of nn interactions to each other, but have fewer AFM interactions than AF3 and AF1 (4 in-plane AFM and 2 out-of-plane AFM). AF2b, which is close in energy to AF4 and AF2a has the same *total* number of nn AFM interactions (six), but they all occur out-of-plane. Finally the FM phase has no AFM interactions, leading to its correspondingly higher energy. By fitting the energies of the six configurations onto the Heisenberg model, we obtained the parameters $J_p = -0.023$ eV and $J_c = -0.028$ eV, with a root mean square deviation of 0.003. The small deviation indicates that a nearest-neighbor Heisenberg model describes the energetics of the system well, and suggests that more distant exchange interactions are weak compared to the nearest-neighbor interactions. Since the Mn-Mn in-plane bond length is almost equal to the out-of-plane Mn-Mn bond length, we obtain $J_p \approx J_c$ as expected.

To conclude this section, we note that AFM coupling is more favourable than FM for both in-plane and out-of-plane Mn-O-Mn bonds and. This suggests that, if doping of Mn ions into ZnO results in clustering of the magnetic ions, we will obtain strong antiferromagnetism.

4.2 Forces and stresses

In many magnetic compounds, a change of magnetic ordering causes a stress which induces a structural distortion [31]. For example, in rocksalt MnO, AFM spin ordering causes a reduction in magnetic symmetry from cubic to rhombohedral, which is accompanied by a structural transition [32]. In some materials, in which there is strong magneto-structural coupling, the distortion can be quite large. For example in CrN the magnetic ordering induces a transition from cubic to orthorhombic symmetry [31, 33, 34]. And in LaMnO₃ the observed A-type antiferromagnetic ordering is unstable in the presence of distortions [35]. The concept of *magnetic stress* has been introduced to describe structural phase transitions that are induced by magnetic ordering [31]. In this section we investigate the magneto-structural coupling in wurtzite MnO, as a precursor to studying the piezoelectric properties in the next Section.

Keeping the lattice parameters of all the structures fixed at the AF3 values, the spin ordering was changed to each of the other five configurations in turn, and the electronic structure was obtained and the stresses and the forces for each magnetic phase were calculated. In the table below, the relative stresses on the unit cell along the z direction and largest forces on the Mn atoms are tabulated for each magnetic ordering.

	AF3	AF1	AF2b	AF4	AF2a
Stress σ_{33} (Ha/bohr ³)	-7.35×10^{-5}	-7.067×10^{-5}	8.35×10^{-5}	-2.39×10^{-4}	-2.46×10^{-4}
Force(max) (Ha/bohr)	5.87×10^{-1}	5.76×10^{-1}	4.42×10^{-3}	8.43×10^{-1}	8.24×10^{-1}

We observe similar groupings as those obtained for the relative energies. The AF1 and AF3

phases are similar in the spin-environment and therefore have similar stresses and forces for the same structure. Likewise, the AF2a and AF4 spin orderings show similar stresses and forces to each other, but both are considerably larger than those in the AF3 and AF1 structures. The significant change in the stress when the magnetic ordering is changed indicates a strong coupling between the magnetic moments of the atoms and the crystal structure.

5 Piezoelectricity

The piezoelectric constant relates the stress response of a material to a uniform electric field or conversely the macroscopic polarization induced by a macroscopic strain. The latter definition is used here to calculate the electro-mechanical response from first principles. We calculated the changes in macroscopic polarization using the Berry phase approach [36] within the ABINIT density functional program [20]. First, the equilibrium structure parameters (a_0 , c_0 and u_0) were obtained for each magnetic configuration, in turn and the spontaneous polarizations, P_0 , (along the z-axis) were calculated. Then the reference structure was strained along the z axis by 1 % ($e_{zz} = 0.01$, e_{zz} is the percentage change in strain along the z-axis) and its structure relaxed with respect to the internal strain (structural parameter u). The polarization P_1 for the relaxed structure was then calculated, and the piezoelectric co-efficient e_{33} was obtained using its definition:

$$e_{33} = \frac{(P_1 - P_0)}{e_{zz}} \quad (2)$$

Subsequent application of a -1% strain along the z-axis showed that the polarization deviated slightly from linearity in MnO (in contrast to ZnO, where it is strictly linear over that range with the same set of convergence parameters.) All the Berry phase polarization calculations used a $2 \times 2 \times 8$ \mathbf{k} -point mesh and a wavefunction tolerance set to 10^{-15} . Calculations for one of the configurations were repeated with a $3 \times 3 \times 8$ mesh to test convergence. A 2×2 mesh in the ab-plane is found to be sufficient as it corresponds to a 4×4 mesh for the primitive unit cell of the wurtzite structure. In order to avoid the Γ point, where the gap vanishes indicating metallicity, the \mathbf{k} -point grid was shifted by $\frac{1}{2}$ along the three co-ordinate axes.

Our calculated values of e_{33} for all the five magnetic orderings are listed in Table 3. While we find groupings of configurations (AF3 and AF1), (AF4 and AF2a) such that the energies and stresses are similar for members of a given group, their piezoelectric constants are found to be somewhat dissimilar, as they are second order derivatives of energy.

The piezoelectric constant of wurtzite MnO in the lowest energy AF3 configuration is about 3 times larger than that of ZnO ($1.0 - 1.2C/m^2$ [3]). In ZnO, the phonon (internal strain) contribution to the piezoelectric constant was found to dominate and this was attributed partly to hybridization between the filled 3d band of Zn and the 2p band of oxygen. In AF3 MnO, we find that the electronic contribution to e_{33} is also significant and in fact has the same sign as that of the phonon contribution (in contrast with ZnO, where the two contributions partially compensate). The large electronic contribution arises because the d band of Mn is only partially occupied and can therefore contribute directly to the piezoelectric response through change in its electron content.

Note that the enhanced piezoelectric response which we find in wurtzite MnO is consistent with earlier observations of large dielectric and piezoelectric constants in systems that are close to electronic and structural instabilities [37]. Wurtzite structure MnO is both unstable structurally (with the rocksalt structure being the ground state) and has other magnetic configurations close in energy. Finally we point out that Mn doped ZnO should have a strong piezoelectric response provided that it remains insulating.

Ordering	AF3	AF1	AF2b	AF4	AF2a
$e_{33}(C/m^2)$	4.81	11.24	0.911	2.05	1.30
$P_0(C/m^2)$	0.045	0.053	0.017	0.014	-0.072

Table 4: Piezoelectric constant, e_{33} and the spontaneous polarization, P_0 , (C/m^2) for the different magnetic orderings of wurtzite MnO.

6 Summary and Conclusions

In this research we investigated the electronic properties of wurtzite MnO using density functional calculations. Using Berry phase polarization calculations we found that magnetic MnO is a stronger piezoelectric than non-magnetic ZnO. This to our knowledge is the first calculation of piezoelectric response in a magnetic material and shows clearly that presence of magnetism does not preclude a piezoelectric response and can even enhance it. The reason for the enhancement is that, in addition to the phonon contribution found in ZnO, the electrons in the partially filled d band of Mn also contribute to the piezoelectricity. Our results suggest that piezoelectricity should persist in Mn doped ZnO provided that it remains insulating. On analyzing the energetics of the different magnetic orderings for wurtzite MnO, however we find that anti-ferromagnetic ordering is more stable than ferromagnetic ordering with the most stable structure having the largest number of nearest neighbor antiferromagnetic interactions. From this we can conclude that if doping of Mn in ZnO results in clustering, ferromagnetism is unlikely.

7 Acknowledgements

This work was supported by the Department of Energy, grant number DE-FG03-02ER45986, and made use of MRL central facilities, supported by the the National Science Foundation under the Award No. DMR00-80034. UVW thanks the Materials Department at the University of California, Santa Barbara for their hospitality.

References

- [1] I.B. Kobiako. *Solid. State. Commun.*, 35:305, 1979.
- [2] A. Dal Corso, M. Posternak, R. Resta, and A. Baldereschi. *Phys. Rev. B.*, 50:10715, 1994.
- [3] N.A. Hill and U.V. Waghmare. *Phys. Rev. B.*, 62:8802, 2002.
- [4] T. Dietl, H. Ohno, F. Matsukura, J. Cibert, and D. Ferrand. *Science*, 287:1019, 2001.
- [5] K. Sato and H. Katayama-Yoshida. *Jpn. J. Appl. Phys.*, 39, 2000.
- [6] K. Sato and H. Katayama-Yoshida. *Phys. Stat. Sol B*, 229:673, 2002.
- [7] K. Ando, H. Saito, Z. Jin, T. Fukumura, Y. Matsumoto, and A. Ohtomo. *Appl. Phys. Lett.*, 78:2700, 2001.
- [8] J.H. Kim, H. Kim, D. Kim, Y.E. Ihm, and W.K. Choo. *Physica B*, 327:304, 2003.
- [9] Z.W. Jin, T. Fukumura, K.Hasegawa, Y.Z. Yoo, K.Ando, T. Sekiguchi, P.Ahmet, T.Chikyow, T. Hasegawa, H. Koinuma, and M. Kawasaki. *J. Crystal Growth*, 237:548, 2002.
- [10] K. Ueda, H. Tabata, and T. Kawai. *Appl. Phys. Lett.*, 79:988, 2001.

- [11] S.W. Lim, D.K. Hwang, and J.M. Myoung. *Solid. State. Commun.*, 125:231, 2003.
- [12] Parmanand Sharma, Amita Gupta, Frank J. Owens K.V. Rao, Renu Sharma, Rajeev Ahuja, J.M. Osorio Guillen, Börje Johansson, and G.A. Gehring. *Nature Materials*, 2:673, 2003.
- [13] A.S. Risbud, N.A. Spaldin, Z.Q. Chen, S. Stemmer, and R. Seshadri. *Phys. Rev. B.*, 68:205202, 2003.
- [14] Nicola Spaldin. *cond-mat/0306477*.
- [15] N.A. Hill. *J. Phys. Chem. B*, 104:6694.
- [16] V. E. Wood and A. E. Austin. in *Magnetoelectric interaction phenomena in crystals*. Gordon and Breach, 1975.
- [17] W.L. Roth. *Phys. Rev. B.*, 110:1333, 1958.
- [18] P. Hohenberg and W. Kohn. *Phys. Rev.*, 136:864, 1964.
- [19] W. Kohn and L.J. Sham. *Phys. Rev.*, 140:1133, 1965.
- [20] X. Gonze *et al.* *ABINIT is a plane wave pseudopotential, a common project of the Universite Catholique de Louvain, Corning Incorporated and other contributors* (URL <http://www.abinit.org>).
- [21] A.M. Rappe, K.M. Rabe, E. Kaxiras, and J.D. Joannopolous. *Phys. Rev. B.*, 41:1227, 1990.
- [22] J.P. Perdew and A. Zunger. *Phys. Rev. B.*, 23:5048, 1981.
- [23] D.M. Ceperley and B.J. Alder. *Phys. Rev. Lett.*, 45:566, 1980.
- [24] W.C. MacKrodt and E.A. Williamson. *J.Phys. Condens. Matter.*, 9:6591, 1997.
- [25] K. Terakura, A.R. Williams T. Oguchi, and J. Kubler. *Phys. Rev. B.*, 30:4734, 1984.
- [26] L.F. Mattheiss. *Phys. Rev. B.*, 5:290, 1972.
- [27] S. Massida, M. Posternak, A. Baldereschi, and R. Resta. *Phys. Rev. Lett.*, 82:430, 1999.
- [28] J.E. Pask, D.J. Singh, and I.I. Mazin. *Phys. Rev. B.*, 64:024403, 2001.
- [29] A. Filippetti and N. A. Spaldin. *Phys. Rev. B.*, 67:125109, 2003.
- [30] R.I. Hines, N.L. Allan, G.S. Bell, and W.C. Mackrodt. *J.Phys. Condens. Matter.*, 9:7105, 1997.
- [31] A. Filippetti and N.A. Hill. *Phys. Rev. Lett.*, 85:5166, 2000.
- [32] S. Massidda *et al.* *Phys. Rev. Lett.*, 82:430, 1999.
- [33] L.M. Corliss, N. Elliott, and J.M. Hastings. *Phys. Rev.*, 117:929, 1960.
- [34] P. Subramanya Herle *et al.*, *J. Solid. State Chem.*, 134:120, 1997.
- [35] D. J. Singh and W. E. Pickett. *Phys. Rev. B.*, 57:88, 1998.
- [36] R.D. King-Smith and D. Vanderbilt. *Phys. Rev. B.*, 47:1651, 1993.
- [37] U. V. Waghmare, N. A. Hill, H. Kandpal, and R. Seshadri. *Phys. Rev. B.*, 67:125111, 2003.